SUPPLEMENTARY INFORMATIONS

for

Synthesis of NiFeOx nanocatalysts from metal-organic precursors for the oxygen evolution reaction

Nguyen Thi Quyen,[1,2,3] Francois Robert, [1,2] Vincent Colliere,[1,2] Pierre Lecante,[4] Karine Philippot,[1,2] Jérome Esvan, [5] Tran Dinh Phong,[3]* Catherine Amiens,[1,2]*

[1] CNRS, LCC (Laboratoire de Chimie de Coordination), 205 Route de Narbonne, BP 44099, F-31077 Toulouse Cedex 4, France.
[2] Université de Toulouse, UPS, INPT, F-31077 Toulouse Cedex 4, France
[3]University of Science and Technology of Hanoi, Vietnam Academy of Science and Technology of Hanoi, 18 Hoang Quoc Viet, Hanoi, Vietnam.
[4]CEMES-CNRS, Université de Toulouse, CNRS, UPS, 29 rue J. Marvig, 31055 Toulouse, France
[5]CIRIMAT, Université de Toulouse, CNRS-INPT-UPS, 4 Allée Emile Monso, BP 44362, 31030 Toulouse, France

1. **Complementary data on the NP characterization.**

a. **Transmission electron microscopy**

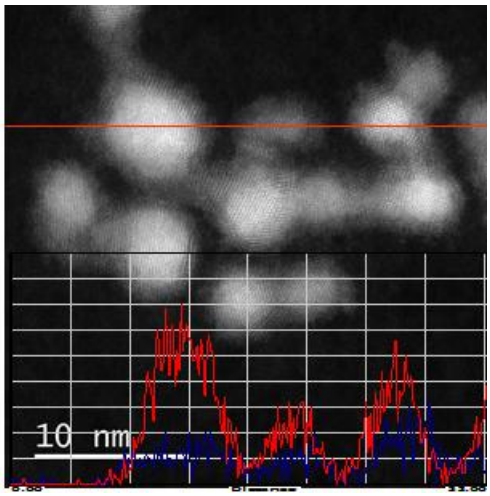

Figure S1. *STEM HAADF (JEM-ARM200F) image of NiFeOx-2/1, and EDX analysis along the horizontal red line: top red and bottom blue curves represent the Fe and Ni contents, respectively.*

a) *b)*

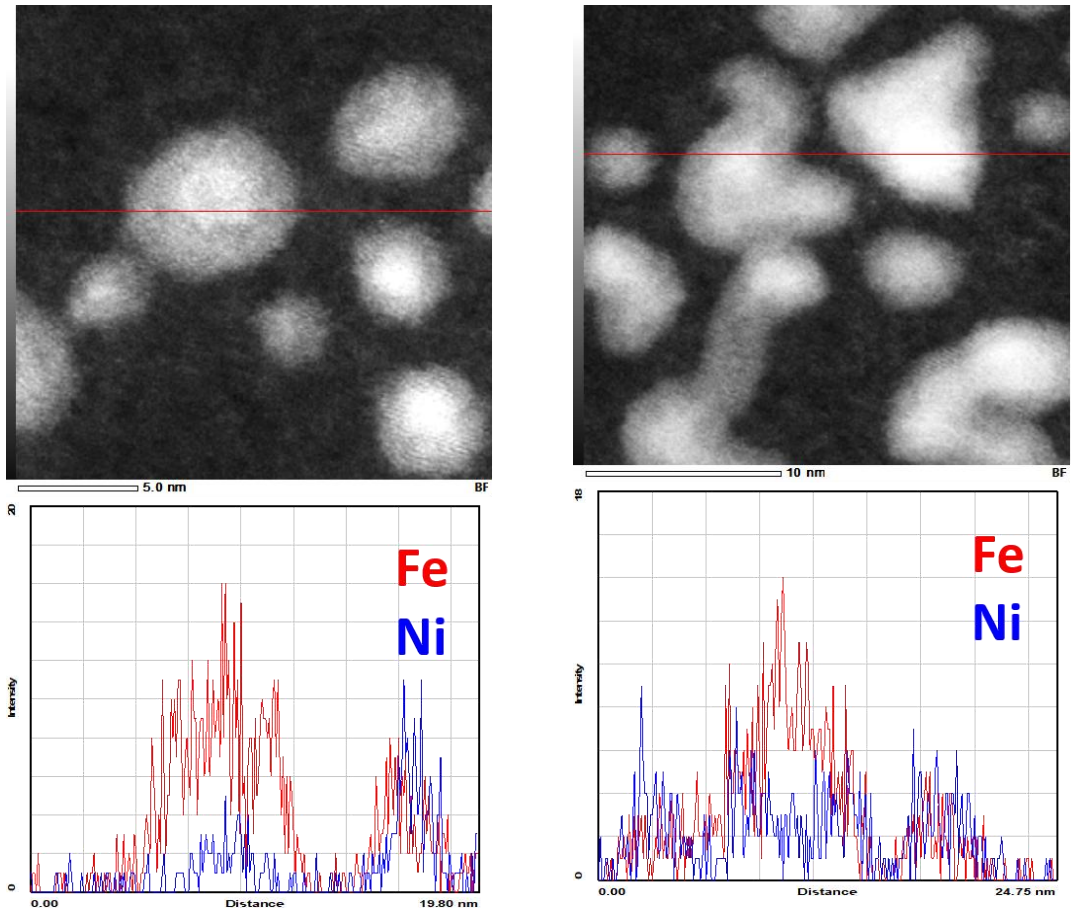

Figure S2. *STEM HAADF (JEMARM200F) images of NiFeOx–1/1 (top) and EDX analysis along the horizontal red line in each image (bottom).*

Figures S1 and **S2** show STEM HAADF images of NiFeOx-2/1 and NiFeOx-1/1 samples (recorded on a JEM ARM200F microscope). Clearly, both Ni and Fe are present in the NPs. Drawing any firm conclusion on the distribution of Ni and Fe inside the NPs is however difficult at such small size, especially as ARM is far from being a statistical method. It can be observed that STEM-EDX analysis of a few NPs from sample NiFeOx–2/1 NPs does not show any clear segregation of the two elements (**Figure S1**). Analysis of sample NiFeOx–1/1 NPs is even less conclusive. Under high resolution imaging conditions, three populations of NPs are evidenced: the smallest spherical NPs, in which no clear segregation of the two elements can be distinguished, the largest spherical NPs which present a surface enriched in Fe (**Figure S2a**), and NPs of irregular shape (**Figure S2b**) showing a shell enriched in Ni. These results must be taken with great care due to lack of statistical data. Indeed the more statistical WAXS investigation shows that most of the NPs comprise a Ni fcc core.

b. Infra-red spectroscopy

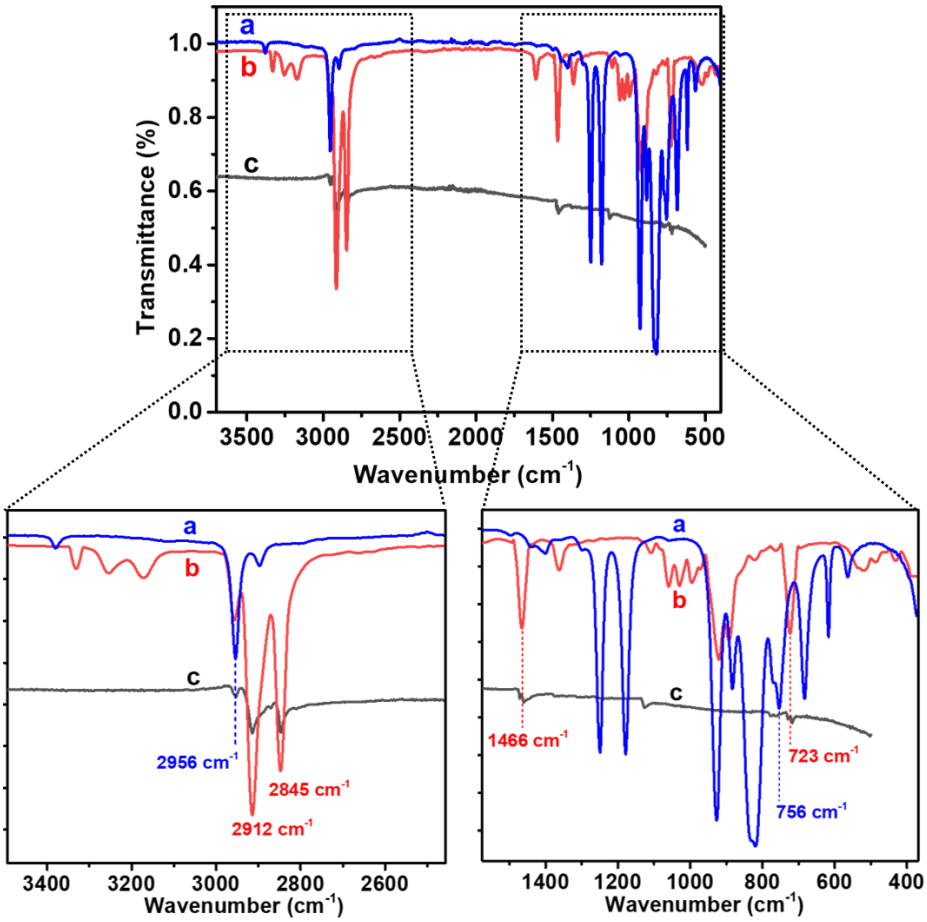

***Figure S3**. FT-IR spectrum of NiFeOx–2/1 (black line, c) compared to reference spectra of HDA (red line, b) and HMDS (blue line, a).*

The two peaks at 2912 cm^{-1} and 2845 cm^{-1} are attributed to vC-H stretching modes of alkyl chains, as in HDA. The peaks at 1466 cm^{-1} and 723 cm^{-1} are attributed to respectively, the CH bending, and CH_2 rocking modes of an alkyl chain, thus confirming the presence of HDA. The absence of peaks in the 1200-800 cm^{-1} region indicates that HMDS, which forms *in situ*[1] is not detected in the powder recovered.

c. Water transfer process

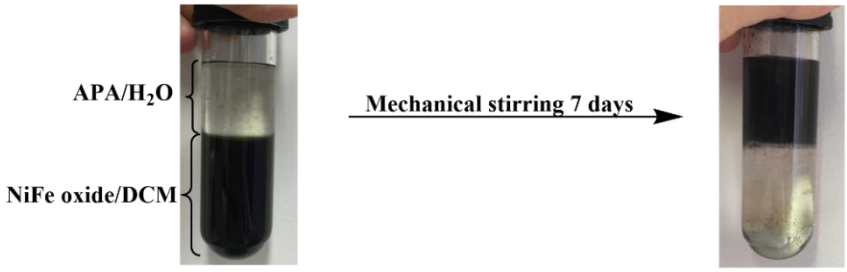

Figure S4. *Pictures of the ligand exchange process.*

2. Synthesis and characterization of the reference samples

Ni and Fe oxide monometallic references were prepared following the synthetic pathways described in **Scheme S1**.

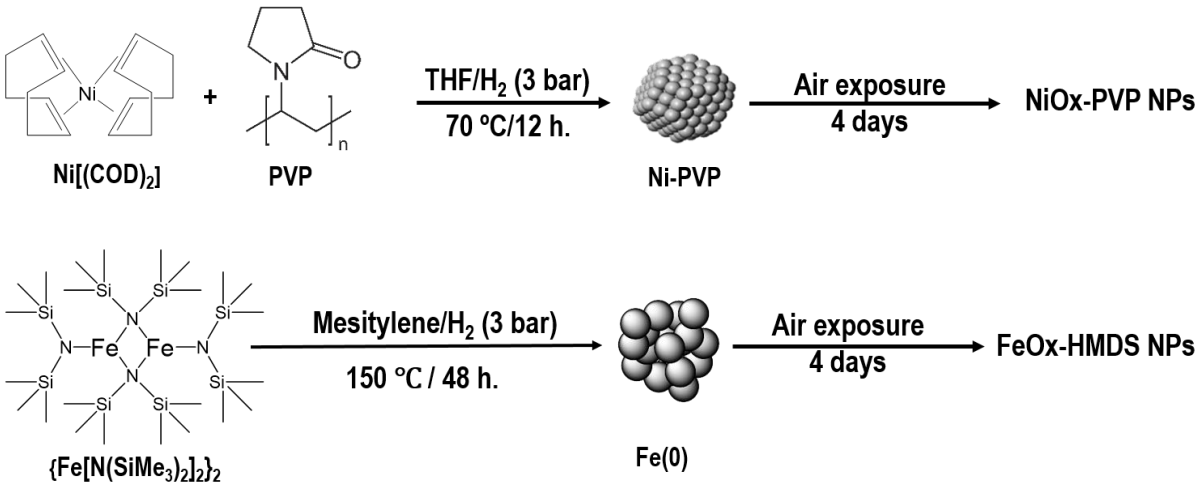

Scheme S1. *Synthesis of Ni (top) and Fe (bottom) oxide reference samples*

Ni[2] and Fe[3] NPs were synthesized following previous publications from our group. Briefly, the Ni NPs were obtained by hydrogenation of the biscyclooctadiene nickel(0) complex (THF, 70 °C, 12 h) in the presence of polyvinylpyrrolidone (PVP) as stabilizer, leading to a nanomaterial with a Ni loading of 9.0 wt% based on ICP-OES data. Fe NPs were synthesized by hydrogenation of the di-bis(bistrimethylsilylamido)iron (II) complex, $[Fe(N(SiMe_3)_2)_2]_2$ (mesitylene, 150 °C, 48 h). The Fe NPs thus obtained are stabilized by HMDS which forms *in situ*. The Fe content determined by ICP-OES is 56 wt%.

As for the NiFe NPs, the as-prepared Ni and Fe NPs were oxidized in air for 4 days, in the solid state. The final nanomaterials are referred to as NiOx-PVP and FeOx-HMDS.

TEM images of NiOx-PVP (**Figure S5a**) revealed the presence of mostly spherical particles with an average size of 3.9 ± 2.1 nm (**Figure S5b**), comparable to that of NiFeOx-2/1-APA and NiFeOx-1/1-APA.

Analysis of the TEM images of FeOx-HMDS indicates that the NPs are also spherical in shape with an average size of 1.6 ± 0.7 nm (**Figure S6**).

a) b)

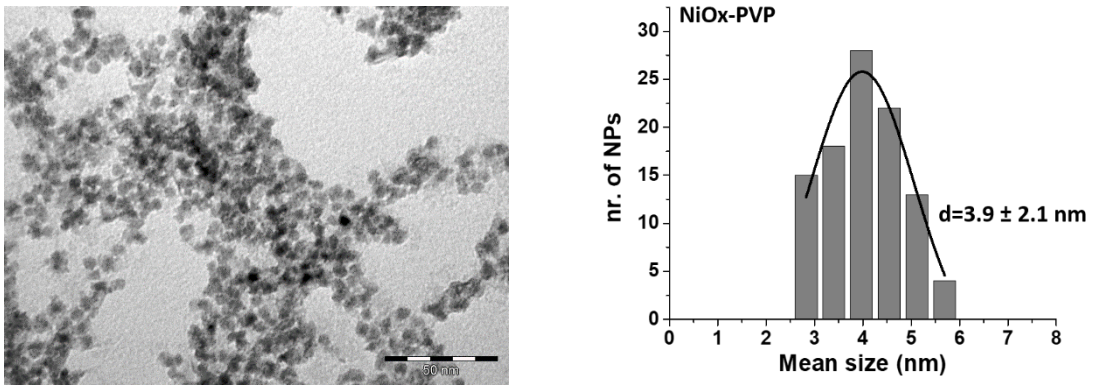

Figure S5*. TEM image of NiOx-PVP (a)(scale bar = 50 nm) and corresponding size histogram (b)*

a)

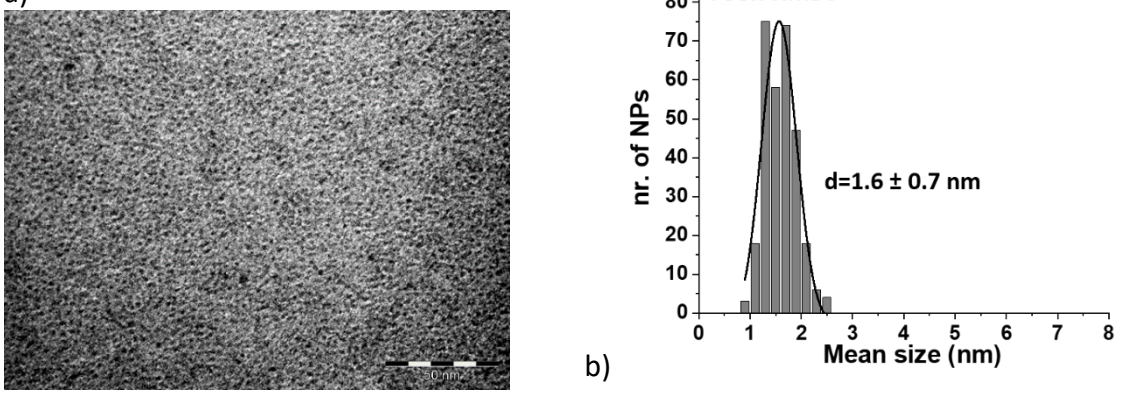

b)

Figure S6*. TEM image of FeOx-HMDS (a)(scale bar = 50 nm) and corresponding size histogram (b).*

a. Structural and electronic characterization of NiOx-PVP :

The sample was analyzed by WAXS to identify the oxide formed (**Figure S7**). Upon oxidation, an increment in the amorphous contribution is noted, but no new diffraction peaks can be observed. Rather, the fcc Ni contribution which is clearly observed in the Ni NPs diagram still dominates the NiOx-PVP diagram. This indicates that oxidation of the Ni NPs in dry conditions produces a passivating amorphous surface layer.

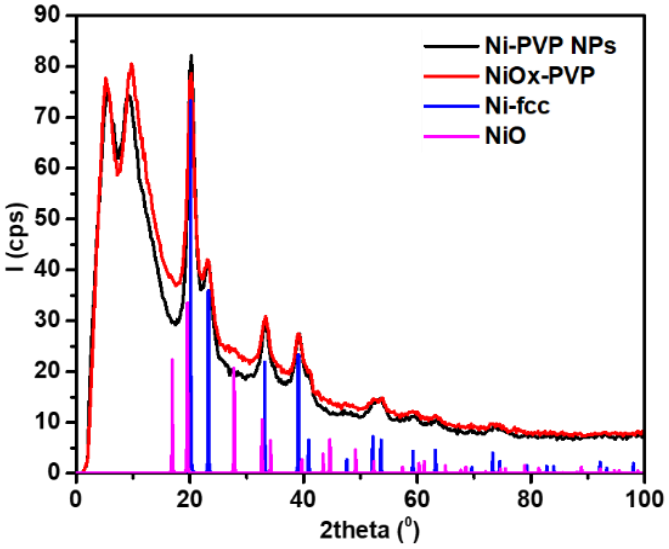

Figure S7. WAXS *diagrams of Ni-PVP reproduced from ref.*[2]*, NiOx-PVP, Ni-fcc (PDF 04-010-6148), and NiO reference pattern (PDF 04-010-6148)*

To identify this amorphous layer, an XPS study was attempted. An aqueous dispersion of the sample was drop casted on a FTO electrode (in conditions used to assess the catalytic activity of the NPs in OER) and studied by XPS. The Ni2p spectrum showed two peaks at 855.9 eV and 861.5 eV which were assigned to Ni^{2+} in a hydroxide environment ($Ni(OH)_2$)(**Figure S8**). No peaks of metallic Ni were found. Given the depth probed by XPS (*circa* 5 nm) and the average size of the NPs (3.9 ± 2.1 nm), this suggests that the passivation afforded by the amorphous surface layer formed upon air oxidation in the solid state was not effective in water. As the NiOx-PVP NPs quickly evolved upon dispersion in water, we thus couldn't identify this first formed amorphous layer. However, this study shows that once deposited on the FTO electrode, the oxidation state of Ni in this sample is comparable to that of Ni at the surface of the NiFeOx-2/1-APA and NiFeOx-1/1-APA nanocatalysts.

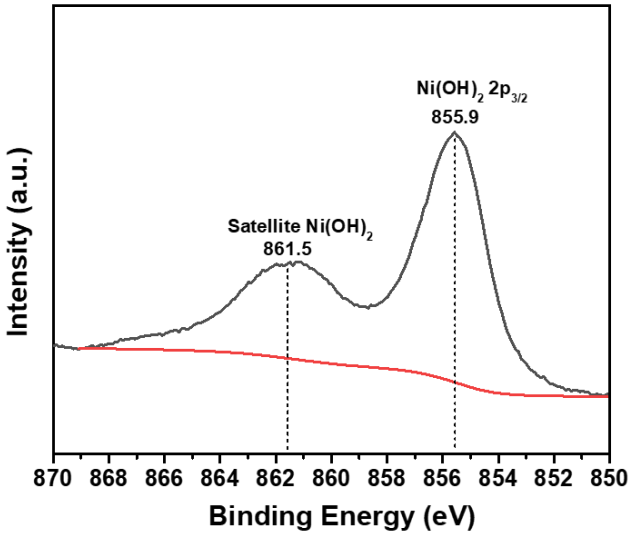

***Figure S8**. Ni 2p XPS spectrum of NiOx-PVP deposited on a FTO substrate.*

b. Structural and electronic characterization of FeOx-HMDS :

WAXS measurements were performed on FeOx-HMDS (**Figure S9**). The Radial Distribution Function calculated from the data displays peaks at 0.19 and 0.32 nm close to the values of the Fe-O and Fe-Fe bonds (in the Fe-O-Fe sequence) that are typical of an oxide. No direct Fe-Fe bonds is observed indicating the full oxidation of the NPs. The size of the crystalline domains is however too small for the structure to be identified unambiguously.

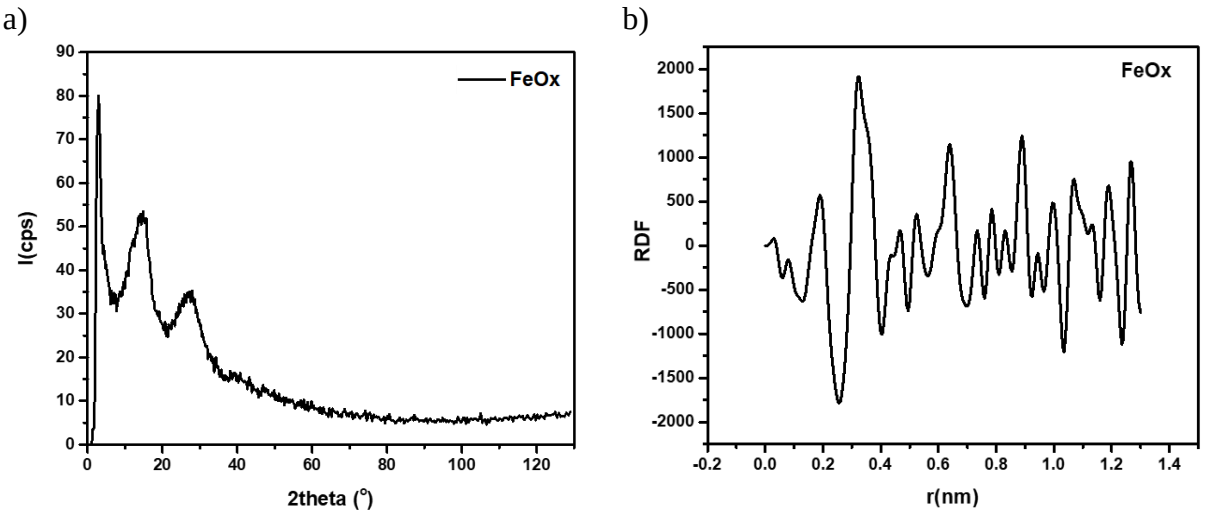

***Figure S9**. a) WAXS diagram and b) RDF of FeOx-HMDS after oxidation in air for 4 days.*

After drop-casting a dispersion of the NPs in a mixture of EtOH/H_2O/Nafion (see experimental part - preparation of catalyst ink) on a FTO support, only one Fe 2p peak can be

observed in the XPS spectrum (**Figure S10**). The binding energy (711.5 eV) corresponds to Fe^{3+} ions like in the oxidized bimetallic NiFeOx-2/1-APA and NiFeOx-1/1-APA nanocatalysts.

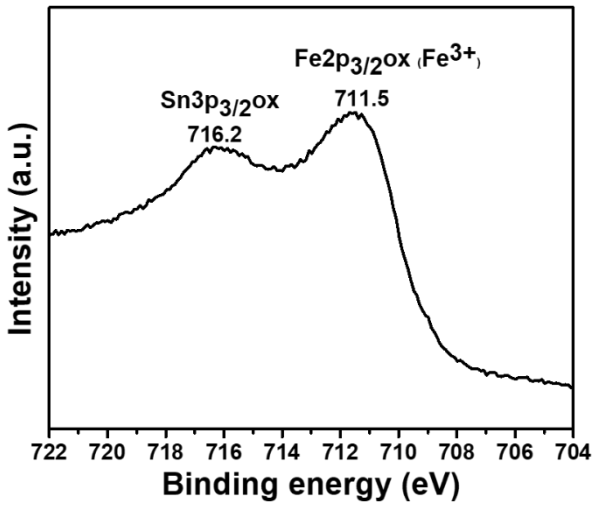

***Figure S10**. Fe 2p XPS spectrum of FeOx-HMDS NPs deposited on FTO.*

3. Details on the synthesis and characterization of NiFeOx-1/9-HMDS

Synthesis of 1Ni/9Fe-HMDS NPs was performed using the adequate ratio of the Ni and Fe precursors, namely 1 $Ni(COD)_2$, 4.5 $[Fe(N(SiMe_3)_2)_2]_2$, and the synthesis pathway used to prepare the reference Fe NPs (**Scheme S1**, bottom). As for the Fe NPs, the final nanomaterial consisted in NPs stabilized by HMDS formed *in situ*.

Once oxidized, the NPs (hereafter referred to as NiFeOx-1/9-HMDS) was characterized by TEM, WAXS and XPS. The TEM image of NiFeOx-1/9-HMDS, **Figure S11a**, shows well dispersed NPs with a mean size of 1.3 ± 0.6 nm (**Figure S11b**) comparable with the average size of the NPs in FeOx.

a) b)

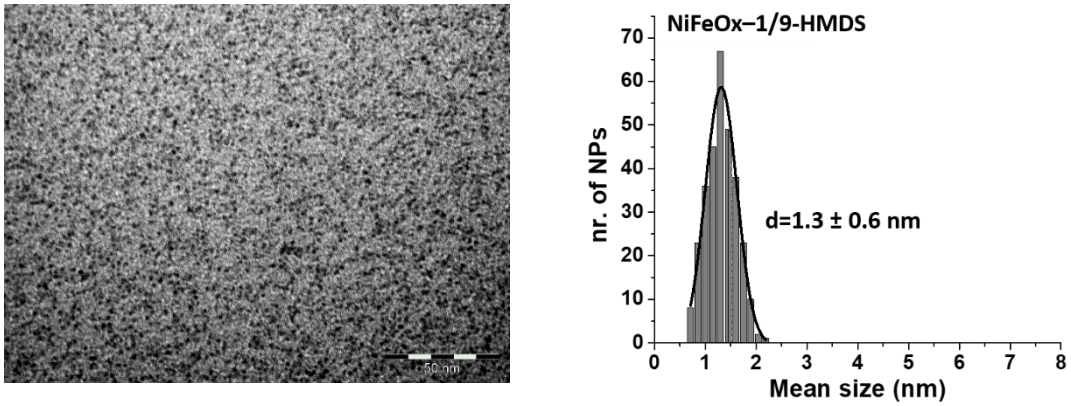

Figure S11. *TEM image of a) NiFeOx-1/9-HMDS (scale bar = 50 nm)and b) corresponding size histogram d = 1.3 ± 0.6 nm.*

Figure S12 shows the WAXS diagrams and RDFs of NiFeOx-1/9-HMDS and FeOx-HMDS. As can be seen from this figure, the structure of NiFeOx-1/9–HMDS presents only a short range order, as in FeOx-HMDS.

a) b)

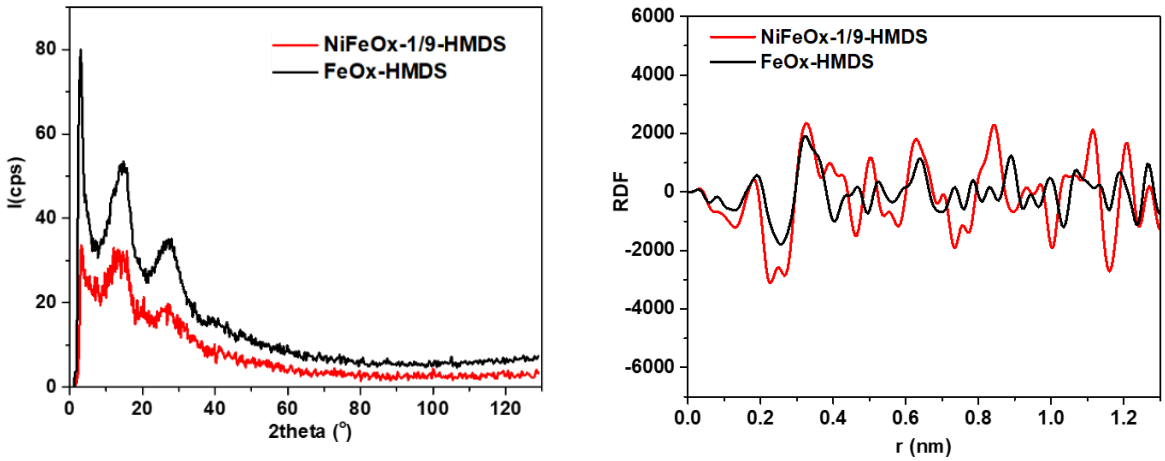

Figure S12. *a) WAXS diagrams and b) RDFs of NiFeOx-1/9-HMDS and FeOx-HMDS*

After drop-casting of a dispersion of the NPs in a mixture of EtOH/H_2O/Nafion (see experimental part - preparation of catalyst ink) on a FTO support the Fe 2p XPS spectrum of NiFeOx-1/9-HMDS presents one peak located at 711.6 eV characteristic of Fe^{3+}(**Figure S13**). The Ni2p spectrum displays a main peak at 856.1 eV attributed to $Ni(OH)_2$. The presence of Ni metal in the sample is ambiguous due to the poor signal/noise ratio in the 852 – 853 eV region (**Figure S14**). The electronic state of Fe and Ni in these NPs is thus similar to the one in the bimetallic NiFeOx-2/1-APA and NiFeOx-1/1-APA nanocatalysts.

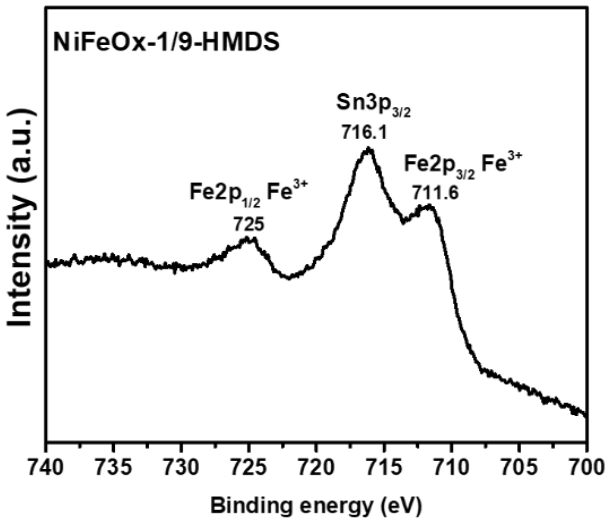

***Figure S13**. Fe 2p XPS spectrum of NiFeOx-1/9-HMDS deposited on FTO*

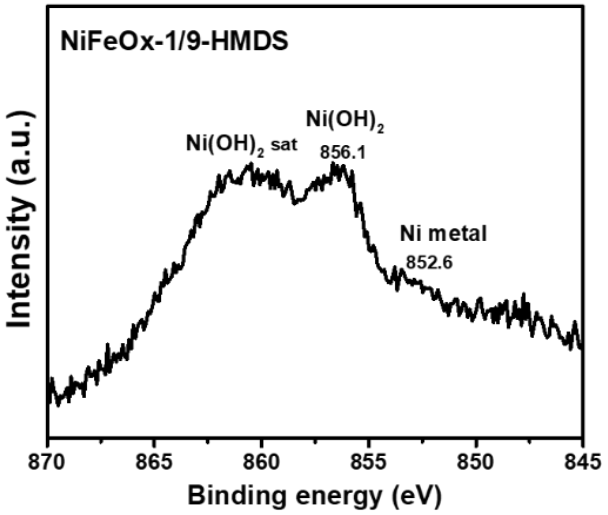

***Figure S14**. Ni 2p XPS spectrum of NiFeOx-1/9-HMDS deposited on FTO*

The Fe and Ni contents were 27 wt% and 3 wt%, respectively, based on ICP analysis. We consider that these NPs consist in an amorphous NiFe oxide of 1Ni9Fe composition bearing only HMDS ligands at their surface.

4. Calculation of TOF values:

The molar amounts of metal atoms (Ni and Fe) in the NiFeOx-2/1-APA and NiFeOx-1/1-APA NPs were determined by ICP-OES analysis, from which the quantity of each element deposited on the electrode could be calculated.

***Table 1**. Details on calculating TOF values for sample NiFeOx-2/1-APA, NiFeOx-1/1-APA, and NiFeOx-1/9-HMDS*

	NiFeOx-2/1-APA	NiFeOx-1/1-APA	NiFeOx-1/9-HMDS
ICP %Ni	63	44	3
ICP %Fe	29	42	27
Concentration of catalyst ink (mg/ml)	3	3	3
Volume deposited (µl)	17	17	17
Mass deposited (mg)	0.051	0.051	0.051
Mol of Fe deposited (mol)	2.64107E-07	3.825E-07	2.45893E-07
Mol of Ni deposited (mol)	5.44576E-07	3.80339E-07	2.59322E-08
Mol of metal atoms deposited (mol)	8.08683E-07	7.62839E-07	2.71825E-07
j at η = 400 mV (mA/cm^2)	26.17	18.27	3.65
I at η = 400 mV (mA)	5.12932	3.58092	0.7154
Mol of O_2 produced (mol)	1.32905E-08	9.27844E-09	1.85366E-09
TOF (s^{-1})	**0.016**	**0.012**	**0.007**

The number of moles of O_2 produced per second was calculated from the current density measured at an overpotential of 400mV, knowing the geometric area of the electrode (0.196 cm^2) and considering that removal of 4 moles of e^- is necessary to produce 1 mole of O_2 (Faraday constant: 96500 C.mol^{-1}; molar mass of Ni taken as 59 g.mol^{-1}, and molar mass of Fe taken as 56 g.mol^{-1}). The turnover number (TOF) was calculated by dividing the number of moles of O_2 produced per second by the total number of moles of metal atoms (following the method of Qiu *et al.*[4]).

5. References

1. O. Margeat, D. Ciuculescu, P. Lecante, M. Respaud, C. Amiens and B. Chaudret, *Small*, 2007, **3**, 451-458.
2. L. Zaramello, B. L. Albuquerque, J. B. Domingos and K. Philippot, *Dalton Trans.*, 2017, **46**, 5082-5090.
3. L.-M. Lacroix, S. Lachaize, A. Falqui, T. Blon, J. Carrey, M. Respaud, F. Dumestre, C. Amiens, O. Margeat, B. Chaudret, P. Lecante and E. Snoeck, *J. Appl. Phys.*, 2008, **103**, 07D521.
4. Y. Qiu, L. Xin and W. Li, *Langmuir*, 2014, **30**, 7893-7901.

6. Abbreviations

APA	3-aminopropyl phosphonic acid
ARM	Atom resolved microscopy
ATR	Attenuated total reflectance
CNTs	Carbon nanotubes
COD	biscyclooctadiene
CVs	Cyclic voltammetrys
DCM	Dichloromethane
EtOH	Ethanol
EDX	Energy dispersive X-ray spectroscopy
FTO	Fluorine-doped tin oxide
FT-IR	Fourier transform infrared
HAADF-STEM	High angle annular dark field-scanning transmission electron microscopy
HDA	Hexadecylamine
HER	Hydrogen evolution reaction
HMDS	Hexamethyldisilazane
HR-TEM	High resolution-transmission electron microscopy
ICP-OES	Inductively coupled plasma-optical emission spectroscopy
LSV	Linear sweep voltammetry
NPs	Nanoparticles
OER	Oxygen evolution reaction
RHE	Reversible hydrogen electrode
SCE	Saturated Calomel Electrode
TEM	Transmission electron microscopy
THF	Tetrahydrofuran
TOF	Turn over frequency
WAXS	Wide angle X-ray scattering
WOCs	Water oxidation catalysts
WS	Water splitting
XPS	X-ray photoelectron spectroscopy